Biochemical and Biophysical Research Communications 503 (2018) 651–656

Contents lists available at ScienceDirect

Biochemical and Biophysical Research Communications

journal homepage: www.elsevier.com/locate/ybbrc

Control of autophagosome size and number by Atg7

Hayley Cawthon [1], Ronith Chakraborty [1], Jacquelyn R. Roberts, Steven K. Backues*

Department of Chemistry, Eastern Michigan University, Ypsilanti, MI, USA

ARTICLE INFO

Article history:
Received 7 June 2018
Accepted 11 June 2018
Available online 18 June 2018

Keywords:
Autophagy
Autophagosome
Autophagic body
Atg7
TEM
Simulation

ABSTRACT

The induction of bulk autophagy by nitrogen starvation in baker's yeast (*S. cerevisiae*) involves the upregulation of many autophagy related proteins, including Atg7. One way to investigate the importance of this upregulation is to measure the size and number of autophagosomes formed when insufficient amounts of that protein are available. Atg8 is known to affect autophagosome size, consistent with its role in phagophore expansion. Atg7 is upstream of Atg8, and might therefore be expected to affect only autophagosome size. We used electron microscopy to measure the size and number of autophagosomes formed with limiting amounts of Atg7 and found them to be both smaller and fewer than normal. This suggests that Atg7 may have an Atg8-independent role in autophagosome initiation in addition to its Atg8-dependent role in autophagosome expansion. We also present an improved simulation for estimating original autophagic body number based on the number of cross-sections observed in ultrathin sections.

1. Introduction

Macroautophagy (hereafter simply "autophagy") is a conserved pathway for trafficking material from the cytoplasm to the vacuole/lysosome for degradation. This material is carried inside double-membrane vesicles termed autophagosomes, which form de novo in the cytoplasm, enveloping their cargo as they form [1]. The outer membrane of the autophagosome then fuses with the vacuole (in yeast and plants) or lysosomes (in animals), so the inner membrane and cargo can be degraded. When the degradative capacity of the yeast vacuole is blocked, the inner membrane and cargo are not broken down, instead accumulating inside the vacuole as autophagic bodies [2]. The size and number of these bodies can be used as a proxy for the size and number of the autophagosomes that were formed [3]. Starvation-induced non-selective autophagy transports bulk cytoplasmic components to the vacuole so that these can be broken down and the nutrients recycled to sustain cellular metabolism [4,5]. When baker's yeast (*S. cerevisiae*) are subjected to nitrogen starvation, they rapidly upregulate autophagy, and within an hour of nutrient withdrawal each cell is forming autophagosomes with an average radius of over 150 nm every 8–10 min [6–8].

Formation of these autophagosomes is accomplished by a suite of Autophagy Related (Atg) proteins, many of which are conserved across eukaryotes. In yeast, most *ATG* genes are upregulated upon nutrient starvation, with *ATG1*, *ATG7*, *ATG8*, *ATG14*, *ATG29* and *ATG41* being some of the most strongly upregulated [9]. In every case so far investigated, levels of these proteins impact overall autophagic flux, which means they must affect either the size or number of autophagosomes formed, or both [7,8,10–12]. Determining which proteins control autophagosome size and which control number not only helps clarify the importance of their expression levels, but also gives insight into their respective roles in the process of autophagosome formation.

The first protein to be studied in this way was Atg8, whose expression increases dramatically upon starvation [8,11]. Insufficient levels of Atg8 lead to a reduction in autophagosome size, but not to autophagosome number [11]. Mutations in Atg8 that lead to reduced autophagic activity or mutations in upstream proteins likewise decrease autophagosome size [13,14]. In contrast, insufficient levels of Atg9 lead to a decrease in autophagosome number, but not to autophagosome size [7]. Atg9 is a transmembrane protein that is trafficked through the secretory pathway to the site of autophagosome formation; mutations in genes necessary for the proper trafficking of Atg9 likewise lead to a reduction in autophagosome number, likely by reducing the amount of Atg9 available for autophagosome formation [12,15–17]. This distinct difference suggests that Atg9 plays an early role, in autophagosome initiation, while Atg8 plays a later role, in expansion of the autophagosome

* Corresponding author.
E-mail address: sbackues@emich.edu (S.K. Backues).
[1] These authors contributed equally to this work.

https://doi.org/10.1016/j.bbrc.2018.06.056
0006-291X/

membrane. This is consistent with other data on the roles of these two proteins [13,18,19], and underlines the information that can be gained from this approach.

Atg8 is a ubiquitin-like protein that is conjugated to the headgroup of phosphatidylethanolamine (PE) in a similar manner to the conjugation of ubiquitin onto other proteins [20]. Like ubiquitin, the conjugation of Atg8 requires an E1 activating enzyme, (Atg7) an E2 conjugating enzyme (Atg3) and an E3 complex that stimulates this activity (Atg12–Atg5) [21]. Atg12 is also an ubiquitin-like protein, and is conjugated to Atg5 by a pathway requiring Atg7 and a different E2 enzyme, Atg10 [22]. Therefore, Atg7 is necessary for the conjugation of two different ubiquitin-like proteins, in both cases contributing to the final goal of attaching Atg8 to the autophagic membrane, where it participates in autophagosome expansion.

Atg7 protein levels increase two-fold upon starvation, and levels of Atg7 have been shown to correlate with overall autophagic flux [10]. Since Atg7 is necessary for Atg8 conjugation, we would hypothesize that Atg7 controls autophagosome size, but not number, just like Atg8. However, in Rph1-overexpressing cells, where induction of Atg7 by starvation is strongly repressed, autophagosomes were found to be the same size, but fewer in number [10]. Rph1 is a transcription factor that controls the expression levels of many genes, so this may be the combined effect of alterations in the levels of multiple Atg proteins. Therefore, it is critical to examine the effect of manipulating Atg7 levels alone, without the manipulation of any other Atg proteins.

2. Methods

2.1. General methods

pRS406 vectors containing protein A-tagged Atg7 (*ATG7-PA*) under the control of distinct promoters were made from their pRS416 counterparts by deletion of the *CEN6* sequence by PCR using phosphorylated primers followed by ligation. Additional details of plasmid and strain construction, growth and western blotting conditions are available in the supplemental methods.

The Pho8Δ60 assay was performed essentially as previously described [23], with the exception that PMSF was omitted in order to avoid interference with the protein quantification, which was performed using a BCA assay (ThermoFisher) in a 96-well plate format with absorbances measured on a BioTek Synergy 2 plate reader.

2.2. TEM analysis

Transmission Electron Microscopy (TEM) and estimation of autophagic body size and number distribution was performed as previously described [24]. In brief, log phase *pep4Δ vps4Δ atg7Δ* cells expressing Atg7-PA under various promoters (or containing just an empty vector with no Atg7-PA) were starved in parallel for 3 h in SD-N, fixed with $KMnO_4$, dehydrated in acetone, embedded in Spurr's resin, sectioned, and systematically imaged at 30,000x for measuring autophagic bodies and 6,000x for measuring vacuoles. Body cross-sections were circled manually and the distribution of the size of these cross-sections was used to estimate the size distribution of the original bodies by numeric methods as described. Similar methods were used to estimate the size of the vacuoles, and additional numeric methods were used to estimate the average number of original bodies based on body size, vacuole size, and the observed number of cross-sections per vacuole.

Additional details of the TEM and image analysis are available in the supplemental methods.

2.3. "R" simulations

Simulation of the sectioning of vacuoles with autophagic bodies was performed in R v 3.4.3 [25] with packages glpkAPI [26] and MultiRNG [27] using successive modifications of the previously published "old (2014)" simulation [24]. The most updated simulation, "Autophagic Body Sectioning Simulation v3.36", referred to here as the "new (2018) simulation", is included in the Supplementary Material as "Simulation Code". This simulation begins by generating a set of spherical vacuoles with lognormal distributed radii based on mu and sigma estimated by numerical methods from measurements of actual vacuoles in that strain. These vacuoles are arranged randomly along the Z axis, and then a 70 nm virtual slice is taken, representing the ultrathin section. Vacuoles not included by the slice are discarded, as are vacuoles where the slice results in a section below the vacuole recognition limit. In vacuoles cut by the slice, autophagic bodies are generated, positioned randomly, and clustered. The radii of the bodies follow a lognormal distribution based on mu and sigma estimated by numerical methods from measurements of actual body sections, and the number of bodies used follows a normal distribution with a given mean and standard deviation. The simulation uses the position of the slice and the clustered bodies to calculate the observed cross-section for each body, discarding any cross-sections smaller than the body recognition limit, and records both the radii of the observed cross-sections and the number of observed cross-sections per vacuole.

The resulting simulated distributions of the number of observed body cross sections per cell were compared to the experimental data, with the goodness of fit measured by the difference between the means and standard deviations of the two data sets and the calculation of the Kolmogorov Smirnov (KS) "D" statistic. The KS test was performed in R v. 3.4.3 b y creating an empirical cumulative density function from the simulated data and comparing the TEM data to it using the command ks. test from the dgof package, which allows use of the one-sample KS test with discrete distributions [28]. Multiple simulations were run, each generating ~4000 measurements, with mean and standard deviation of the number of original bodies systematically varied, starting with a mean equal to the to the value estimated from the numerical methods and a range of standard deviations. We looked for values that minimized both measures of goodness of fit; this typically occurred over a small range of means (within one or two) and a slightly larger range of standard deviations (within three to five).

3. Results

3.1. Atg7 controls both autophagosome size and number

To examine the effect of altering the levels of Atg7, we created yeast strains expressing C-terminally protein A (PA)-tagged Atg7 under the control of various promoters in a *Pho8Δ60* background. The promoters chosen were the same ones used previously [10], however, we chose to integrate our constructs into the *URA3* locus to give stable transformants instead of expressing them on centromeric plasmid [10]. We felt this would give the most consistent results when using TEM to measure the size and number of autophagosomes formed in each cell, as centromeric plasmids can vary in copy number from cell to cell [29].

We integrated *ATG7-PA* under the control of ~800bp of the native *FLO5*, *GAL3* and *SEF1* promoters into a pho8Δ60, *atg7Δ* strain to measure autophagic activity. Western blotting verified that these strains gave a wide range of Atg7 expression levels, with the *SEF1* promoter yielding mild overexpression, *GAL3p* a 10-fold underexpression, and *FLO5p* a 50-fold underexpression (Fig. 1A).

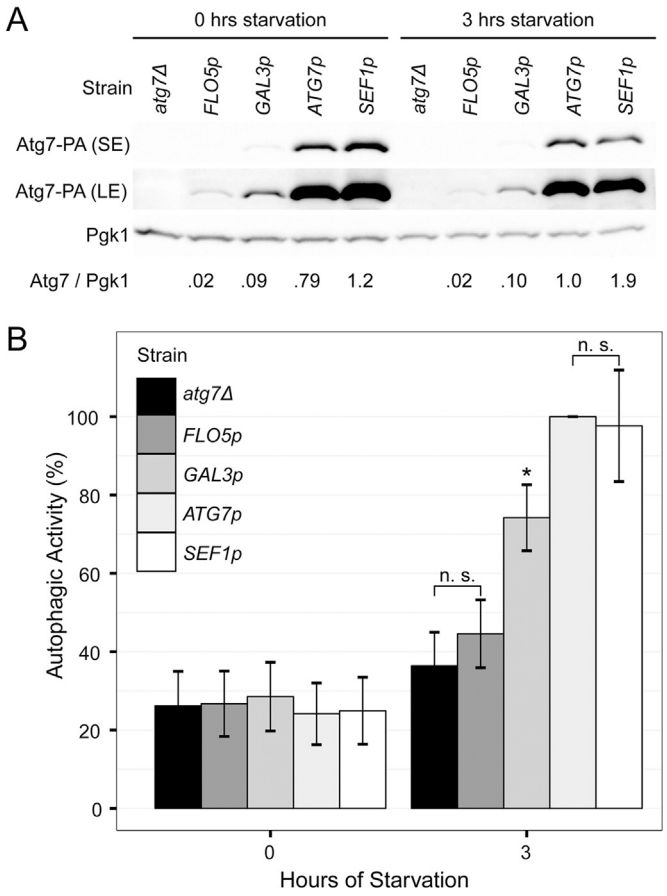

Fig. 1. ATG7 levels control the amount of autophagy.
(A) Protein levels of Atg7-PA expressed under different promoters in a *pho8Δ60* background during growing conditions ("0 h") and after 3 h of nitrogen starvation. A short (SE) and long (LE) exposure of the PA blot are shown. The Atg7/Pgk1 values shown are the average of six biological replicates and are normalized to the *ATG7p* 3-h signal. (B) Autophagic activity of the strains from (A) measured by the Pho8Δ60 assay. $N \geq 10$ biological replicates, with each replicate independently normalized to the *ATG7p* 3-h timepoint. Error bars = 95% CI. * = $p < 0.05$ compared to all other samples; n. s. = not significant ($p > 0.05$).

Pho8Δ60 assay verified that underexpression of Atg7 leads to a reduction in autophagic activity under nitrogen starvation conditions: the *GAL3* promoter led to a ~40% reduction in autophagic activity, while the *FLO5* promoter gave levels of autophagic activity that were indistinguishable from background (Fig. 1B). Interestingly, the *SEF1* promoter did not result in increased autophagy, suggesting that native Atg7 levels are not rate-limiting for autophagy. All of these results are consistent with those reported previously, with the exception that the integrated strains used in this study provided ~5 fold lower levels of expression for the *GAL3* and *FLO5* promoters than centromeric plasmids used previously, which may be why we did not see the small but measurable amount of autophagic activity reported for the *FLO5* promoter [10].

With our methodology verified, we integrated these constructs into a strain lacking vacuolar protease activity and the multivesicular body pathway (*pep4Δ*, *vps4Δ*, *atg7Δ*) so we could visualize the autophagic bodies by TEM. We omitted the *SEF1p* overexpression strain as its autophagic activity was equal to the native promoter, but included the *FLO5p* underexpression strain because TEM is more sensitive for detecting autophagy than the Pho8Δ60 assay. We verified the levels of Atg7-PA in these strains by western blotting (Fig. 2A), then analyzed the size and number of autophagic bodies accumulated after 3 h of nitrogen starvation by TEM (Fig. 2B). The observed size and number of the autophagic body cross-sections (Fig. 2C–D) were used to estimate the actual size distribution and average number of autophagic bodies in each strain using an established numerical estimation method [24]. Reduced levels of Atg7 led to a reduction in both the size and the number of autophagic bodies generated (Fig. 2E–F and Supplemental Table 1). The *GAL3p* strain, which had ~25% as much Atg7 protein as the *ATG7p* strain, was estimated to generate about 70% as many bodies with an average volume about half that of the native *ATG7p* strain.

3.2. Refinement of simulation methods for autophagic body number

We noticed that cells from the *FLO5p* strain showed a variable number of autophagic body cross-sections per vacuole section: 57% of vacuole sections contained no visible bodies, while 1.6% showed 10 or more bodies. Some variability is expected due to the bodies clustering together in the vacuole: if a given section does not pass through the cluster, no body cross-sections will be seen, while if it happens to pass through the center of the cluster, many will be seen. However, we wondered whether this was sufficient to explain the extreme variability of observed body cross-sections in these samples, or whether additional explanations were necessary. To answer this, we used a simulation developed to model the sectioning of autophagic bodies in a vacuole [24]. Unlike the numerical methods used for Fig. 2E–F, the simulation includes the clustering of the bodies in the vacuole, therefore giving an estimate of the expected distribution of observed bodies per vacuole section.

The original simulation randomly generates a given number of bodies within a vacuole of a fixed size, clusters them, and takes a random slice through the vacuole (bounded by the minimum observable vacuole section size) [24]. However, actual yeast vacuoles vary with cell size, which follows approximately a lognormal distribution [30,31]. Therefore, we estimated the distribution of vacuole sizes in each strain using the same methods used to estimate the distribution of body sizes. Body number was systematically varied using a normal distribution to determine which values gave the best fit.

The results from new simulation ("2018") with variable vacuole size and body number were compared to the old simulation ("2014") with fixed vacuole size and body number. As expected, both simulations still gave the same results for the size distribution of the body cross-sections, which is already a good match to the experimental data (Supplemental Fig. 1). However the new simulation gave a distribution of observed bodies per cell that was more similar to the experimental TEM data, even when body number was held constant (Fig. 3A–B). Allowing the original number of bodies per vacuole to vary between cells gave a still better fit to the experimental data (Fig. 3C). Using this improved simulation, we estimated that cells expressing Atg7 under the native *ATG7* promoter produced 38 ± 4 autophagic bodies after 3 h of starvation, while those expressing lower levels of Atg7 (*GAL3p*) produced 26 ± 15, and those expressing the lowest levels of Atg7 (*FLO5p*) produced 16 ± 2. The standard deviations in these estimates are not a not a measurement of error, but instead an estimate of cell-to-cell variability in body number. Interestingly, their values do not support the hypothesis that the number of autophagic bodies *FLO5p* samples is fundamentally more variable than in *ATG7p* samples, instead suggesting that most of the variation can be explained by the clustering of the bodies and random sampling of the vacuole.

4. Discussion

We found that insufficient levels of Atg7 resulted in both smaller and fewer autophagic bodies presumably reflecting the formation

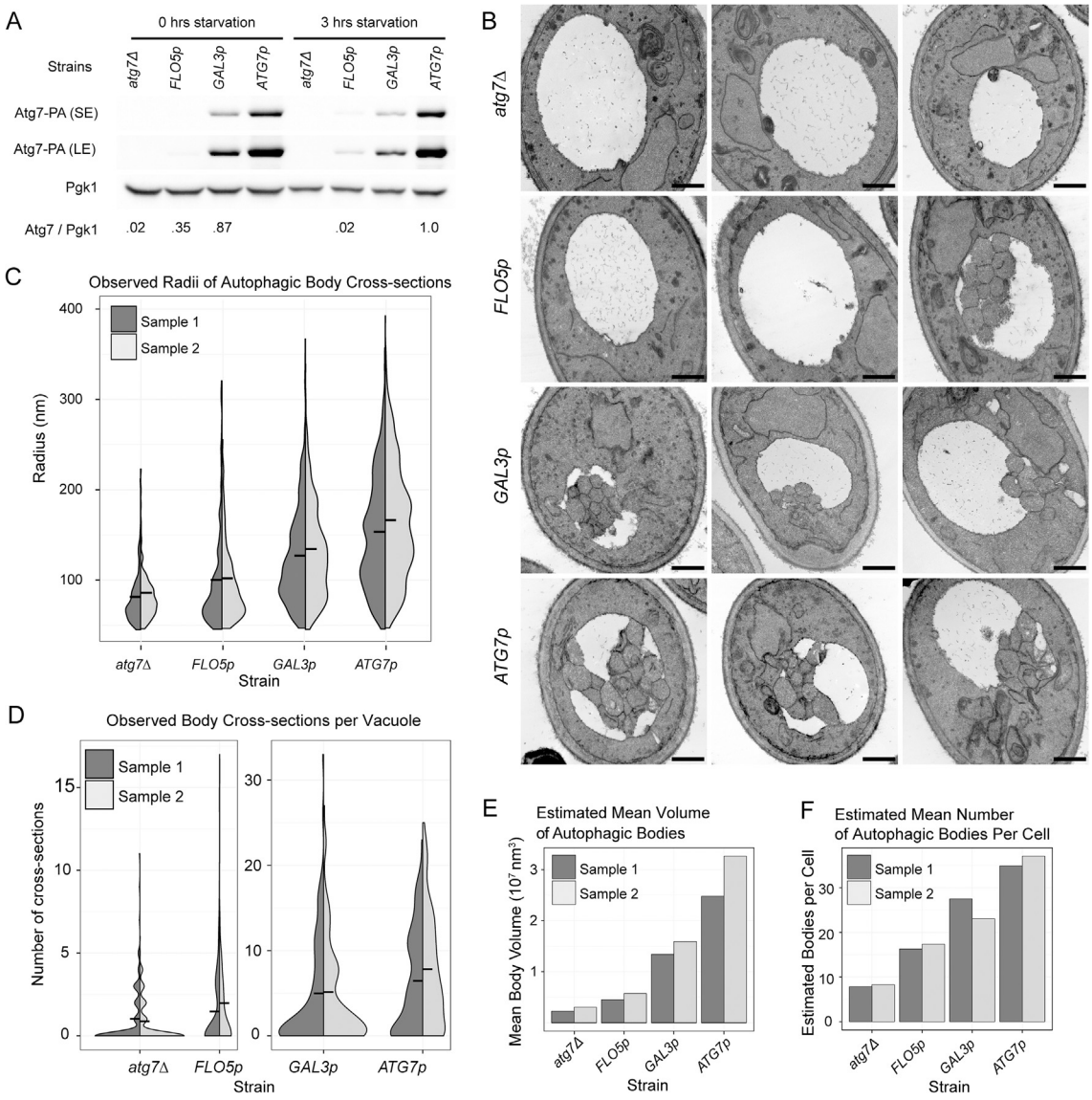

Fig. 2. ATG7 levels control both autophagosome size and number.
(A) Protein levels of Atg7-PA in cultures used for TEM during growing conditions ("0 h") and after 3 h of nitrogen starvation. A short (SE) and long (LE) exposure of the PA blot are shown. The Atg7/Pgk1 values shown are the quantification of the short exposure of this blot. (B) TEM images of *pep4Δ vps4Δ atg7Δ* strains expressing Atg7-PA under the indicated promoters or with just an empty vector ("*atg7Δ*") after 3 h of nitrogen starvation. The *pep4Δ* mutation blocks the degradative capacity of vacuole, thus preserving the autophagic bodies, while *vps4Δ* additionally blocks the multivesicular body pathway. Three representative images of each strain represent the range of observed bodies. Scale bars = 600 nm. (C) Split violin plots showing the distribution of observed cross sectional radii of the autophagic bodies seen in TEM sections from each strain. Horizontal bars indicate the mean radius. "Sample 1" and "Sample 2" represent different sets of cultures grown and processed on different days. N > 100 bodies from >100 cells per strain per sample. (D) Split violin plots showing the distribution of the number of autophagic body cross-sections seen in a given cell cross-section in TEM sections from each strain. Horizontal bars indicate the mean number of body cross-sections per cell. (E) Mathematical methods were used to estimate the original lognormal distribution of body sizes that would have resulted in the observed distribution of body section radii (Supplemental Table 1); the mean volume of the bodies was calculated from each estimated original distribution. (F) Mathematical methods that take into account the size of the bodies in each strain were used to estimate the original number of autophagic bodies in each cell that would have given rise to the average number of observed body cross-sections per cell. Cells expressing higher levels of Atg7-PA contained both more and larger autophagic bodies.

of fewer and smaller autophagosomes. The effect on size is greater, with strains expressing less Atg7 showing greater reductions in autophagosome size than in autophagosome number. Both the original estimation methods and the improved simulation gave similar results for average autophagic body number, and the newer simulation allowed an estimate of the variation in body number from cell to cell. The *FLO5p* sample could not be fit as well with the simulated data, perhaps because the smaller number of bodies seen in that case allowed more interference from the background of non-Atg7-dependent structures in the vacuole. Nevertheless, it was clear that the *FLO5p* sample, like the *GAL3p* sample, showed both fewer and smaller autophagic bodies, demonstrating that Atg7 levels control both autophagosome number and autophagosome size. This result is in contrast to what has been shown for Atg8, where insufficient levels lead only to smaller autophagosomes, not fewer. Similarly, a mutation that reduces the function of Atg3, which acts directly downstream of Atg7 in Atg8 lipid conjugation, primarily affects autophagosome size [14].

Atg7 is involved in two conjugation pathways: the conjugation of Atg8 to PE, and the conjugation of Atg12 to Atg5. The established function for the Atg12–Atg5 conjugate in yeast autophagy is enhancing the lipidation of Atg8 [21,32]. The fact that Atg7 affects

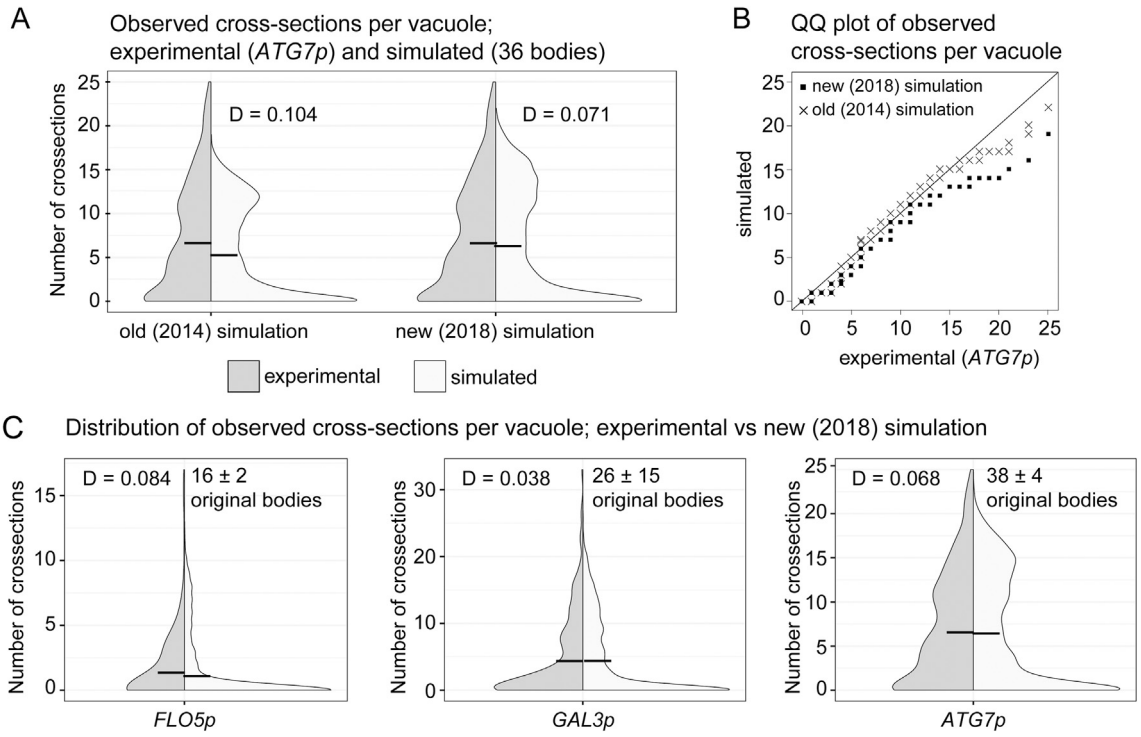

Fig. 3. Refinement of the simulation program gives a better estimate of autophagosome number.
(A) Comparison of the distribution of observed body sections per vacuole from the *ATG7p* TEM data (dark gray) with that predicted by the old (2014) or new (2018) simulations (light gray). Horizontal bars indicate the mean number of body cross-sections per cell. A better fit is indicated by lower values of D, calculated using the Kolmogorov–Smirnov test. (B) QQ plot of the TEM data vs both the old and the new simulations. A better fit is indicated by points that more closely follow the diagonal line, as is seen for the new simulation. (C) Split-violin plots of to the best fit results from the new (2018) simulation (light gray) compared to the actual TEM data (dark gray). Parameters used in the simulation are listed in Supplemental Table 2; N ≥ 200 actual and 3000 simulated cells. A better fit was obtained for the *ATG7p* and *GAL3p* samples than for the *FLO5p* samples, but all fits were better with than with the old 2014 simulation.

both autophagosome size (expansion) and number (nucleation) while Atg8 affects only expansion suggests that Atg7 may have additional, Atg8-independent, roles in autophagosome formation, perhaps via the Atg12–Atg5 conjugate. Indeed, a recent in vitro study demonstrated that Atg12–Atg5 in complex with Atg16 has membrane tethering activity, and suggested that this may have a role in autophagosome initiation [33]. This is a possible explanation of the effect of Atg7 on autophagosome number; the investigation of additional proteins in this pathway by the same methods used here should clarify this point.

A role for Atg7 in controlling autophagosome number was first hinted at in a study of the transcriptional repressor Rph1, the overexpression of which inhibits the induction of *ATG7* expression during starvation, along with that of various other *ATG* genes. Rph1 overexpression causes a >50% decrease in autophagosome number without any effect on autophagosome size [10]. Since Atg7 reduction affects both autophagosome size and number, the repression of *ATG7* alone is not a sufficient explanation for the effects of Rph1 overexpression; the repression of other *ATG* genes must compensate for the effect on autophagosome size while perhaps contributing to the effect on autophagosome number.

Acknowledgements

Thanks to Dr. Dan Klionsky of the U of M Life Sciences Institute for much generous help, including plasmids and advice. Thanks to the Eastern Michigan University (EMU) Department of Chemistry for both financial and intellectual support, in particular Dr. Ross Nord for suggestions on refining the simulation. Thanks to Dr. Kathy Chu of the EMU Department of Mathematics for advice on appropriate statistical tests and to EMU student Pat Wall for help with error handling in R. Thanks to Dr. Thomas Mast and the EMU Biology Department for use of their equipment for preparing ultrathin sections for TEM, and to the U of M MIL for use of their TEM. Funding was provided by the NSF (RUI grant #1613653 to S. K. Backues) and the EMU Provost's office.

Appendix A. Supplementary data

Supplementary data related to this article can be found at https://doi.org/10.1016/j.bbrc.2018.06.056.

Transparency document

Transparency document related to this article can be found online at https://doi.org/10.1016/j.bbrc.2018.06.056.

References

[1] Z. Xie, D.J. Klionsky, Autophagosome formation: core machinery and adaptations, Nat. Cell Biol. 9 (2007) 1102–1109.
[2] K. Takeshige, M. Baba, S. Tsuboi, T. Noda, Y. Ohsumi, Autophagy in yeast demonstrated with proteinase-deficient mutants and conditions for its induction, J. Cell Biol. 119 (1992) 301–311.
[3] Z. Xie, U. Nair, J. Geng, M.B. Szefler, E.D. Rothman, et al., Indirect estimation of the area density of Atg8 on the phagophore, Autophagy 5 (2009) 217–220.
[4] Z. Yang, J. Huang, J. Geng, U. Nair, D.J. Klionsky, Atg22 recycles amino acids to link the degradative and recycling functions of autophagy, Mol. Biol. Cell 17 (2006) 5094–5104.
[5] J. Kaur, J. Debnath, Autophagy at the crossroads of catabolism and anabolism, Nat. Rev. Mol. Cell Biol. 16 (2015) 461–472.
[6] M. Baba, K. Takeshige, N. Baba, Y. Ohsumi, Ultrastructural analysis of the autophagic process in yeast: detection of autophagosomes and their characterization, J. Cell Biol. 124 (1994) 903–913.

[7] M. Jin, D. He, S.K. Backues, M.A. Freeberg, X. Liu, et al., Transcriptional regulation by Pho23 modulates the frequency of autophagosome formation, Curr. Biol. 24 (2014) 1314–1322.
[8] Z. Xie, U. Nair, D.J. Klionsky, Atg8 controls phagophore expansion during autophagosome formation, Mol. Biol. Cell 19 (2008) 3290–3298.
[9] G. Hu, T. McQuiston, A. Bernard, Y.-D. Park, J. Qiu, et al., A conserved mechanism of TOR-dependent RCK-mediated mRNA degradation regulates autophagy, Nat. Cell Biol. 17 (2015) 930–942.
[10] A. Bernard, M. Jin, P. González-Rodríguez, J. Füllgrabe, E. Delorme-Axford, et al., Rph1/KDM4 mediates nutrient-limitation signaling that leads to the transcriptional induction of autophagy, Curr. Biol. 25 (2015) 546–555.
[11] C.R. Bartholomew, T. Suzuki, Z. Du, S.K. Backues, M. Jin, et al., Ume6 transcription factor is part of a signaling cascade that regulates autophagy, Proc. Natl. Acad. Sci. Unit. States Am. 109 (2012) 11206–11210.
[12] Z. Yao, E. Delorme-Axford, S.K. Backues, D.J. Klionsky, Atg41/Icy2 regulates autophagosome formation, Autophagy 11 (2015) 2288–2299.
[13] H. Nakatogawa, Y. Ichimura, Y. Ohsumi, Atg8, a ubiquitin-like protein required for autophagosome formation, mediates membrane tethering and hemifusion, Cell 130 (2007) 165–178.
[14] M. Sakoh-Nakatogawa, H. Kirisako, H. Nakatogawa, Y. Ohsumi, Localization of Atg3 to autophagy-related membranes and its enhancement by the Atg8-family interacting motif to promote expansion of the membranes, FEBS Lett. 589 (2015) 744–749.
[15] K.A. Tucker, F. Reggiori, W.A. Dunn, D.J. Klionsky, Atg23 is essential for the cytoplasm to vacuole targeting pathway and efficient autophagy but not pexophagy, J. Biol. Chem. 278 (2003) 48445–48452.
[16] W.-L. Yen, J.E. Legakis, U. Nair, D.J. Klionsky, Atg27 is required for autophagy-dependent cycling of Atg9, Mol. Biol. Cell 18 (2007) 581–593.
[17] K. Meiling-Wesse, F. Bratsika, M. Thumm, ATG23, a novel gene required for maturation of proaminopeptidase I, but not for autophagy, FEMS Yeast Res. 4 (2004) 459–465.
[18] K. Suzuki, Y. Kubota, T. Sekito, Y. Ohsumi, Hierarchy of Atg proteins in pre-autophagosomal structure organization, Gene Cell. 12 (2007) 209–218.
[19] H. Yamamoto, S. Kakuta, T.M. Watanabe, A. Kitamura, T. Sekito, et al., Atg9 vesicles are an important membrane source during early steps of autophagosome formation, J. Cell Biol. 198 (2012) 219–233.
[20] Y. Ohsumi, Y. Ichimura, T. Kirisako, T. Takao, Y. Satomi, et al., A ubiquitin-like system mediates protein lipidation, Nature 408 (2000) 488–492.
[21] T. Hanada, N.N. Noda, Y. Satomi, Y. Ichimura, Y. Fujioka, et al., The Atg12-Atg5 conjugate has a novel E3-like activity for protein lipidation in autophagy, J. Biol. Chem. 282 (2007) 37298–37302.
[22] Y. Ohsumi, N. Mizushima, T. Noda, T. Yoshimori, Y. Tanaka, et al., A protein conjugation system essential for autophagy, Nature 395 (1998) 395–398.
[23] T. Noda, D.J. Klionsky, Chapter 3 the quantitative Pho8Δ60 assay of nonspecific autophagy, Methods Enzymol. 451 (2008) 33–42.
[24] S.K. Backues, D. Chen, J. Ruan, Z. Xie, D.J. Klionsky, Estimating the size and number of autophagic bodies by electron microscopy, Autophagy 10 (2014) 155–164.
[25] R. R Core Team, A language and environment for statistical computing. https://www.r-project.org/, 2017.
[26] G. Gelius-Dietrich, glpkAPI: R Interface to C API of GLPK. https://cran.r-project.org/package=glpkAPI, 2015.
[27] H. Demirtas, R. Allozi, MultiRNG: multivariate pseudo-random number generation. https://cran.r-project.org/package=MultiRNG, 2018.
[28] T.A. Arnold, J.W. Emerson, Nonparametric goodness-of-fit tests for discrete null distributions, Rev. Javer. 3 (2011) 34–39.
[29] A.S. Karim, K.A. Curran, H.S. Alper, Characterization of plasmid burden and copy number in Saccharomyces cerevisiae for optimization of metabolic engineering applications, FEMS Yeast Res. 13 (2013) 107–116.
[30] Y.-H.M. Chan, W.F. Marshall, Organelle size scaling of the budding yeast vacuole is tuned by membrane trafficking rates, Biophys. J. 106 (2014) 1986–1996.
[31] A.K. Bryan, A. Goranov, A. Amon, S.R. Manalis, Measurement of mass, density, and volume during the cell cycle of yeast, Proc. Natl. Acad. Sci. Unit. States Am. 107 (2010) 999–1004.
[32] Y. Cao, H. Cheong, H. Song, D.J. Klionsky, In vivo reconstitution of autophagy in Saccharomyces cerevisiae, J. Cell Biol. 182 (2008) 703–713.
[33] J. Romanov, M. Walczak, I. Ibiricu, S. Schüchner, E. Ogris, et al., Mechanism and functions of membrane binding by the Atg5-Atg12/Atg16 complex during autophagosome formation, EMBO J. 31 (2012) 4304–4317.